Supporting Information for

Direct observation of charge inversion in divalent nanofluidic devices

Sylvia Xin Li[1*], Weihua Guan[2], Benjamin Weiner[1], Mark Reed[3*]

1. Department of Physics, Yale University
2. Department of Electrical Engineering, Pennsylvania State University
3. Department of Electrical Engineering & Applied Physics, Yale University

*E-mail: xin.li.xl288@yale.edu, mark.reed@yale.edu

1. Device Setup

2. The pH Measurement

3. Open Potential Measurements and Error Analysis

4. Numerical Model

5. Conductance Measurements and Error Analysis

6. Strongly Correlated Liquid (SCL) Theory

1. Device Setup

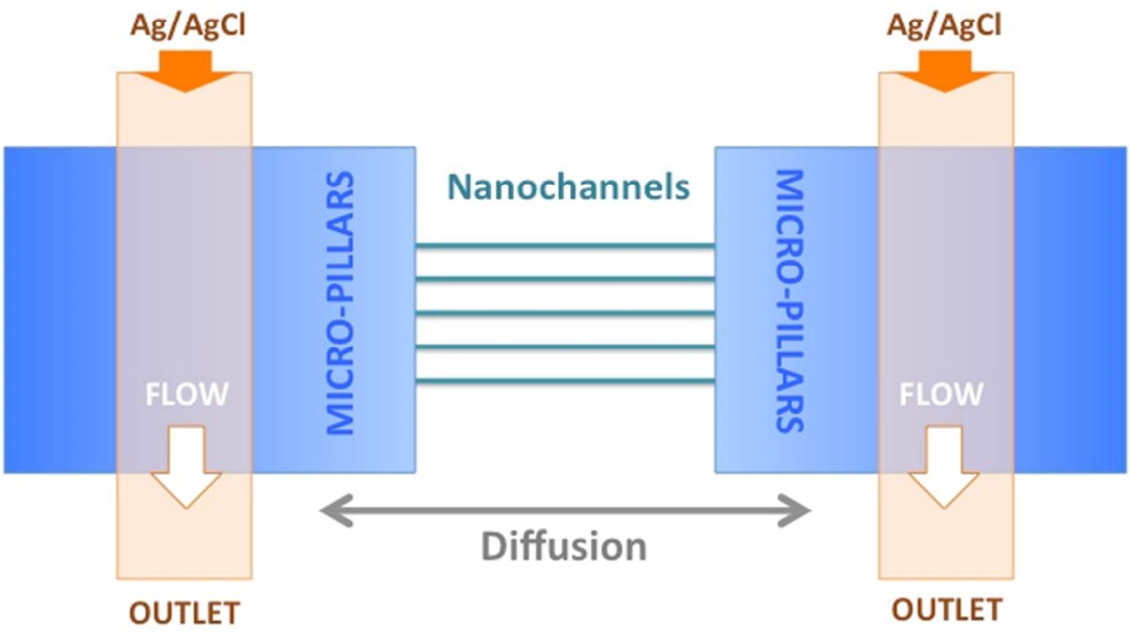


Figure S1

Figure S1: The device schematic of flow direction and diffusion area

The Ag/AgCl electrodes are fabricated by standard electrochemistry methods by coating AgCl on Ag wires. The electrodes are then inserted in the flow inlets, while the outlets are inserted with waste tubes. The solutions are pumped into the microfluidic channels inside PDMS (the orange layer), and then diffuse into the micro-pillar region where the microfluidic channels overlap with this transition region (the micro-pillar region). The solution will further diffuse into the nanochannels. The transition micro-pillar region also serves as an effective filter of random dust inside the solution with pillar size and space separation both of ~3μm.

2. The pH Measurement

The pH of an electrolyte solution affects many electrochemical properties of interest, such as the conductance and open potential. We measured the pH of our solutions over various time intervals in order to more accurately incorporate pH into our model. We found that the pH depends on the time elapsed since the electrolyte solution was mixed. For both KCl and $MgCl_2$, the final pH reaches 5.0±0.3 and therefore all the solutions for the measurement are used when they reach the saturation pH. All measurements are carried out using the Omega PHB-600R pH meter.

To minimize pollution, the pH probe was rinsed using de-ionized (DI) water then immersed into the solution, where it was held stationary by clamp until the digital reading stabilized. The probe was rinsed with DI water and then the process was repeated. In the time between measurements, solutions were stored in sealed containers with limited access to air.

$MgCl_2$ pH Measurements				
Concentration (Mol)	Concentration\time Δt	1 hour	2 hours	1 week
	5.1E-08	5.6	5.5	5
	5.6E-07	5.6	5.4	5
	6.2E-06	5.4	5.9	5.3
	6.8E-05	5.1	5.7	5
	0.00075	5.1	6	5.1
	0.00826	5.2	5.1	5
	0.09091	5.1	4.9	4.9
	1	4.7	4.6	4.7

Table S1

It is seen that over long time periods the pH tends to decrease, and that higher concentrations of $MgCl_2$ have slightly lower pH. This is to be expected because $MgCl_2$ is a Lewis acid that allows hydronium (H_3O^+) to form in solutions. We also carried out measurements on KCl solution and DI water. The DI water's pH is 5.7 after a day and decays to 5.1 after 1 week.

KCl pH Measurements			
Concentration (Mol)	Concentration\time Δt	1 day	1 week
	10^-6	5.1	5
	10^-5	5.3	4.8
	10^-4	5.6	4.9
	10^-3	6.6	4.9
	10^-2	6	4.8
	10^-1	5.4	4.8
	1	5.3	4.9

Table S2

Therefore, the pH we later use in the numerical model is 5.

3. Open Potential Measurements and Error Analysis

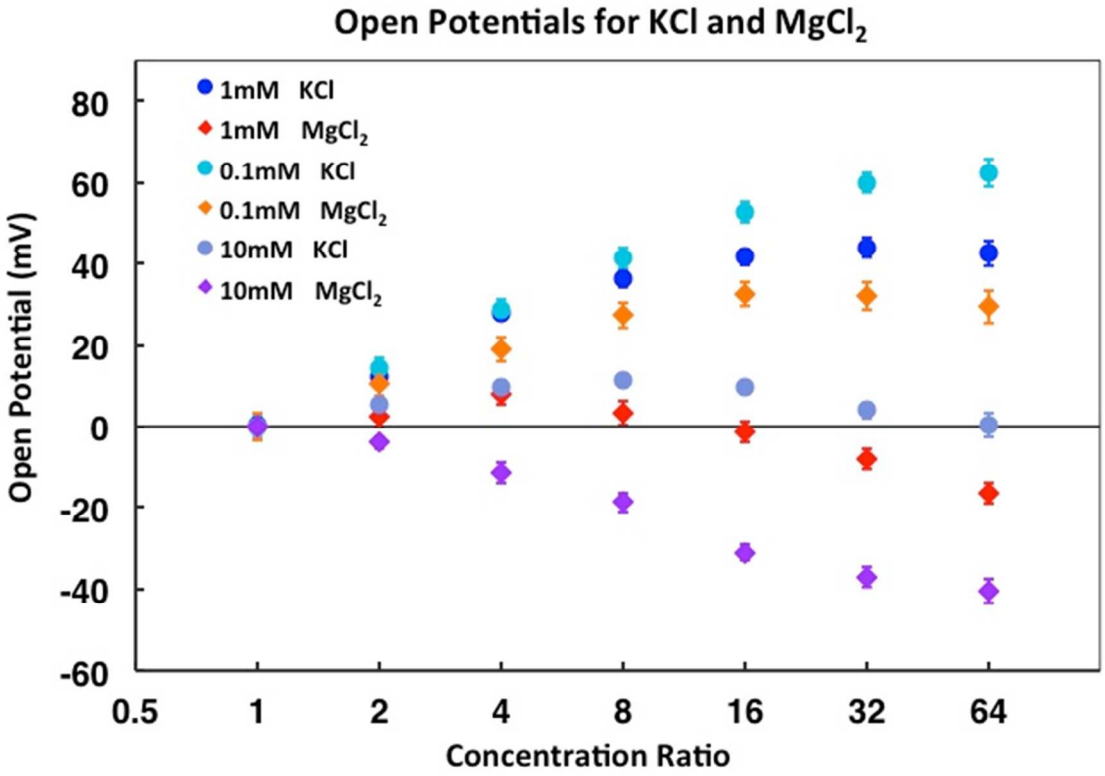


Figure S2

Figure S2: Open potentials of KCl and $MgCl_2$ in three concentration series, with the *cis* end fixed concentration of 0.1mM, 1mM and 10mM, and concentration ratio of *trans/cis* from 1 to 64 in binary logarithm.

The *cis* end of nanochannels has a fixed concentration of 0.1mM, 1mM or 10mM. The *trans/cis* concentration ratio varies from 1 to 64 in binary logarithm. In the plotted open potential graph, we have accounted for the electrode potential that arises from different solution concentrations, independently of the nanochannels. According to the reversible reaction AgCl $\Leftrightarrow$ $Ag^+ + Cl^-$ at the Ag/AgCl electrodes, we can apply Nernst equation $\psi = \frac{RT}{F} * \ln(C_{\text{trans}}/C_{\text{cis}})$ to the electrode potential and represent the open potential by the equation of $\Phi = V_{\text{measure}} - \psi$, where V_{measure} is the measured overall potential. Buffer solutions are avoided to minimize the number of ion species in the nanochannel system. Figure S2 shows all the open potentials measured in both monovalent (KCl) and divalent ($MgCl_2$) cases. Each data point has been measured at least 3 times. The fluctuation of open potential can possibly result from the following reasons: 1) The electrode potential is fluctuating, we tested the electrode potential of different concentrations connected by salt bridge and the fluctuations from the expected value vary from 1mV to 3mV; 2) The

equilibrium state of nanochannels is not stable, especially when the concentration ratio is higher.

4. Numerical Model

To interpret the surface charge from open potential, we propose a comprehensive model of coupled partial differential equations, which can be solved numerically to simulate the behavior of our experiments. This numerical solution not only explains our experimental data but also can be used as a general transport model in nanofluidic systems. Our model treats the nanochannel as two separate regions: i) a thin layer at the very surface of channel/solution walls where screening and charge inversion occur; ii) a diffuse layer where the familiar Poisson equation:

$$\nabla^2 V = -\sum_i Z_i C_i F/\varepsilon$$

This relates the electric potential to a given space charge density represented by ion concentrations (Z_i is the ion valence, C_i the concentration and F the Faraday constant). If the equilibrium state follows a Boltzmann distribution, the well-known Poisson-Boltzmann equation can be solved. An alternative approach describes the dynamic process of ionic flux using the Nernst-Planck equation (as in our numerical model):

$$\nabla * (-D_i \nabla C_i - Z_i F C_i \mu_i \nabla V) = 0$$

The denotation *i* represents the ion species (K^+ or Mg^{2+}, Cl^-, H^+ and HCO_3^-).

Meanwhile, the complicated surface layer can be regarded as a boundary of net surface charge to the diffuse region. The electric potential, ion concentrations, and the net surface charge are then coupled together and the goal of interpreting the net surface charge from open potential can be realized. The calculated average net surface charge inside the channel plotted in Figure 2 and 3 in the main part of the paper is defined by assuming the net surface charge along the nanochannel doesn't have gradient. We define a 2D area for numerical simulation in COMSOL script environment: 20nm high and 5μm long nanochannel connecting two square reservoirs with edge length of 3μm shown in Figure S1.



Figure S3

Figure S3: The area definition in numerical simulation

A more detailed model would describe the gradient of potential inside the nanochannels and takes into account the change of net surface charge along the nanochannel. Since SiO_2 is well understood, we can refer to the literature to estimate the dissociation constant pK (usually 6-7) and maximum density of total SiOH groups Γ_{SiOH} (8/nm^2). [1]-[2] The bare surface charge density of SiO^- is characterized as:

$$\sigma = e\frac{\Gamma_{SiOH}10^{-pK}}{10^{-pK}+[H^+]}$$

Here $[H^+]$ is the local proton concentration and e is the elementary charge. Counterions of positive cations are attracted to the negative bare surface charge and the attraction of the closest layer is so strong that these counterions are not as mobile as those as diffuse layer, thus forming the Stern layer. The Stern layer counterions not only contribute to the net surface charge as a screening layer, but also influence the local pH and the dissociation constant. [1] This leads to the question of whether screening could be strong enough that the Stern layer charge compensates or even exceeds the bare surface charge. For strong screening, we introduce a screening factor β so that the net surface charge would be expressed as $(1-\beta)\sigma$, whereas at low concentrations β is close to zero and can be neglected. The accuracy could further be improved by adjusting the dissociation constant related to the specific kind of cation species and different concentration ranges. For the low concentration range (below 1mM), we couple the Poisson-Nernst-Planck (PNP) equations with a changeable net surface charge model based on the surface chemistry by assuming the charge inside Stern layer can be neglected.

It is further shown in Fig. 8 that an average net surface charge could be used (as mentioned before) in the numerical simulation to produce results consistent with the dissociation model, demonstrating that our model yields the expected behavior in low concentrations. Therefore, we can estimate the net surface charge for the higher concentration of $MgCl_2$, where the net surface charge inverts sign. This same numerical model could be used for conductance simulation in the range of low concentrations with concentration ratio =1.

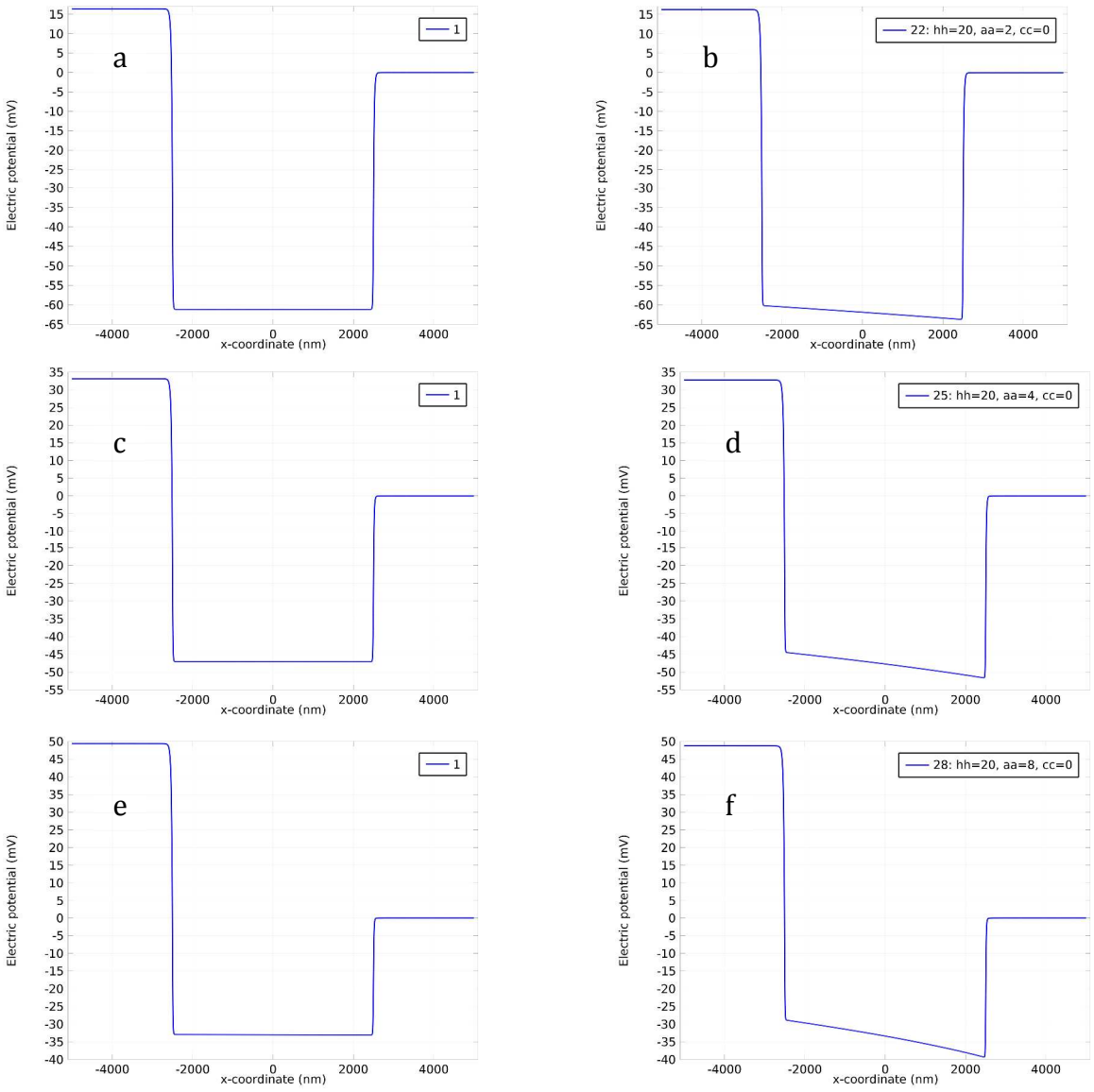


Figure S4

Figure S4: Simulation comparison between average surface charge model (a, c, e) and changing surface charge model (b, d, f) for *cis*= 0.1mM KCl, concentration ratio of 2(a, b), 4(c, d) and 8(e, f)

5. Conductance Measurements and Error Analysis

The conductance measurement error mostly comes from the electrode potential drift (<=20mV) and the noise of current at very low concentrations (<=0.01mM). When the concentration is higher than 0.01mM, the potential drift decreases to less than 10mV. But since our voltage sweep is from -0.5V to 0.5V, the overall fluctuation of conductance is within 10%. The following is charts of simulation results we used in Figure 4, the improved model for low concentration conductance. This numerical model is described in the previous session.

$MgCl_2$ with SiOH maximum group density 8/nm^2 and SiOH dissociation constant pK = 6.1:

Concentration (mM)	Surface charge density (mC/m^2)	Mg^{2+} (mM/m^3)	H^+ (mM/m^3)	Cl^- (mM/m^3)	HCO_3^+ (mM/m^3)	Conductance (1.0E-11 S)
2.00E-05	-1.04	0.13015	0.81307	4.85E-07	1.21E-04	6.321599799
3.00E-05	-1.09	0.17579	0.77158	7.67E-07	1.28E-04	6.322633221
5.00E-05	-1.17	0.24808	0.71006	1.39E-06	1.39E-04	6.285289884
8.00E-05	-1.27	0.32943	0.64689	2.44E-06	1.53E-04	6.240124578
1.00E-04	-1.32212	0.37294	0.61562	3.21E-06	1.61E-04	6.188564087
2.00E-04	-1.53	0.52775	0.51771	7.65E-06	1.91E-04	6.021689039
3.00E-04	-1.67	0.63181	0.46243	1.29E-05	2.14E-04	5.864526705
5.00E-04	-1.89	0.77733	0.3972	2.50E-05	2.50E-04	5.705018666
8.00E-04	-2.13	0.92617	0.34265	4.64E-05	2.90E-04	5.581860283
1.00E-03	-2.24968	1.00216	0.31876	6.25E-05	3.12E-04	5.517847687
0.002	-2.69	1.26221	0.25286	1.58E-04	3.95E-04	5.428446018
0.003	-2.99	1.43283	0.21995	2.73E-04	4.55E-04	5.443197141
0.005	-3.41	1.66972	0.18393	5.46E-04	5.46E-04	5.533472763
0.006	-3.57	1.76074	0.17244	7.00E-04	5.84E-04	5.584035214
0.007	-3.72	1.84051	0.16324	8.64E-04	6.17E-04	5.650622528
0.008	-3.85	1.91178	0.15565	0.00104	6.48E-04	5.709094431
1.00E-02	-4.07417	2.03556	0.1437	0.00141	7.03E-04	5.819067408
2.00E-02	-4.86	2.46035	0.11187	3.63E-03	9.09E-04	6.304170695
3.00E-02	-5.39	2.74109	0.09653	6.34E-03	1.06E-03	6.693383745
0.05	-6.12	3.13267	0.0801	0.01281	0.00128	7.275084492
0.08	-6.87	3.53617	0.06742	0.02449	0.00153	7.916922862
0.1	-7.26238	3.74424	0.06212	0.03331	0.00167	8.267748105
0.2	-8.6	4.47211	0.04815	0.08665	0.00217	9.505804175
0.5	-10.74	5.69686	0.03446	0.30599	0.00306	11.58013852
0.8	-12.03	6.50801	0.02912	0.58145	0.00363	12.86156399

Table S3

KCl with SiOH maximum group density 8/nm^2 and SiOH dissociation constant pK = 6.8:

Concentration (mM)	Surface charge density (mC/m^2)	K^+ (mM/m^3)	H^+ (mM/m^3)	Cl^- (mM/m^3)	HCO_3^+ (mM/m^3)	Conductance (1.0E-11 S)
2.00E-05	-0.42984	8.77E-04	0.4383	4.54E-07	2.27E-04	2.95E+00
3.00E-05	-0.43004	0.00131	0.43808	6.81E-07	2.27E-04	2.95E+00
5.00E-05	-0.43045	0.00219	0.43763	1.14E-06	2.27E-04	2.95E+00
8.00E-05	-0.43107	0.0035	0.43696	1.82E-06	2.28E-04	2.95E+00
1.00E-04	-0.43147	0.00437	0.43651	2.28E-06	2.28E-04	2.947185324
2.00E-04	-0.43351	0.00869	0.43429	4.58E-06	2.29E-04	2.938234998
3.00E-04	-0.43553	0.01297	0.43211	6.91E-06	2.30E-04	2.929364653
5.00E-04	-0.43954	0.02139	0.42784	1.16E-05	2.33E-04	2.912168333
8.00E-04	-0.44549	0.03374	0.42166	1.89E-05	2.36E-04	2.887439539
0.001	-0.4494	0.04177	0.41768	2.38E-05	2.38E-04	2.871656327
0.002	-0.46842	0.07987	0.39929	4.98E-05	2.49E-04	2.800129281
0.003	-0.48661	0.11493	0.38307	7.79E-05	2.60E-04	2.739216097
0.005	-0.52083	0.17783	0.35565	1.40E-04	2.79E-04	2.641308785
0.008	-0.56779	0.25876	0.32344	2.46E-04	3.07E-04	2.53630088
0.01	-0.59676	0.30613	0.30613	3.24E-04	3.24E-04	2.48540251
0.02	-0.72195	0.49492	0.24746	8.02E-04	4.01E-04	2.352312259
0.03	-0.82549	0.63764	0.21254	0.0014	4.67E-04	2.315473043
0.05	-0.99521	0.85627	0.17125	0.0029	5.79E-04	2.340441818
0.08	-1.19678	1.10157	0.13769	0.00577	7.21E-04	2.452819574
0.1	-1.30977	1.23513	0.12351	0.00805	8.05E-04	2.540487854
0.2	-1.74179	1.73473	0.08673	0.02301	0.00115	2.96830401
0.3	-2.05825	2.09934	0.06997	0.04295	0.00143	3.335630053
0.5	-2.53081	2.65861	0.05317	0.09493	0.0019	3.927364691

Table S4

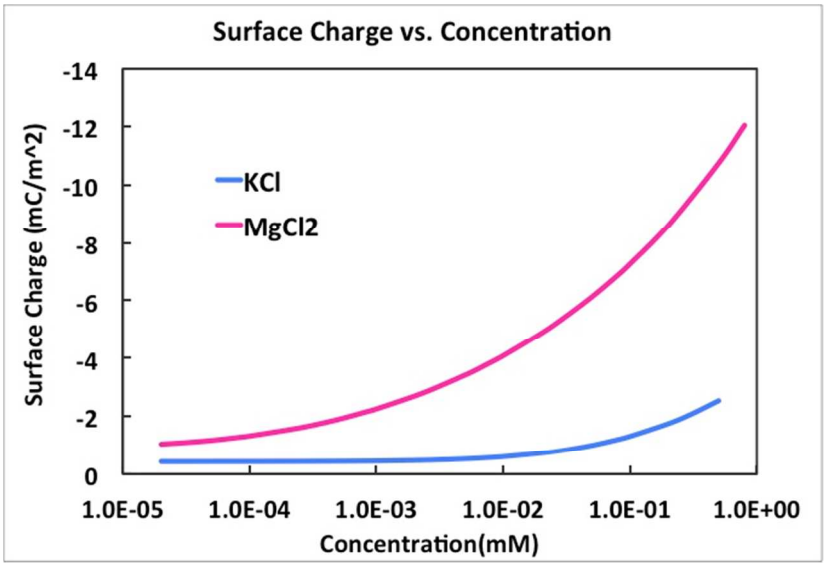


Figure S5

Figure S5: Surface Charge of KCl and $MgCl_2$ under low concentration range

The bulk conductivity of $MgCl_2$ and KCl were measured with a commercial conductivity meter and the nano/bulk conductivity ratios and the divalent/monovalent conductivity ratios are plotted in the following graphs:

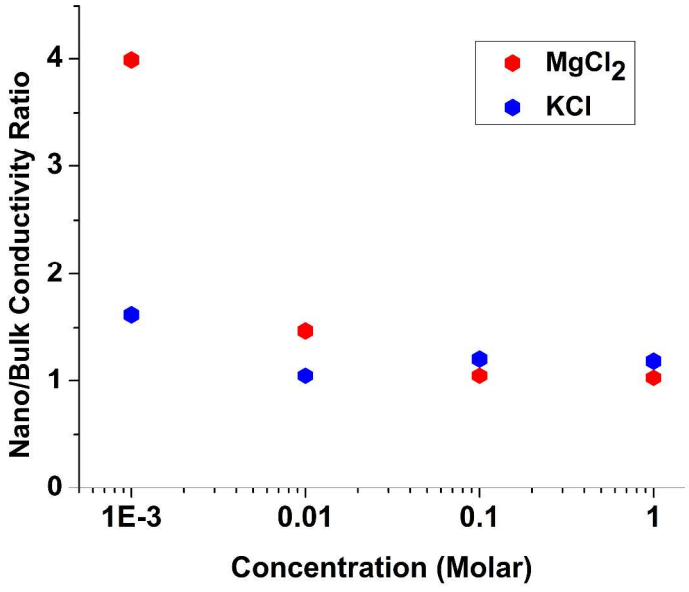


Figure S6

Figure S6: Nano/Bulk conductivity ratio plotted against concentration

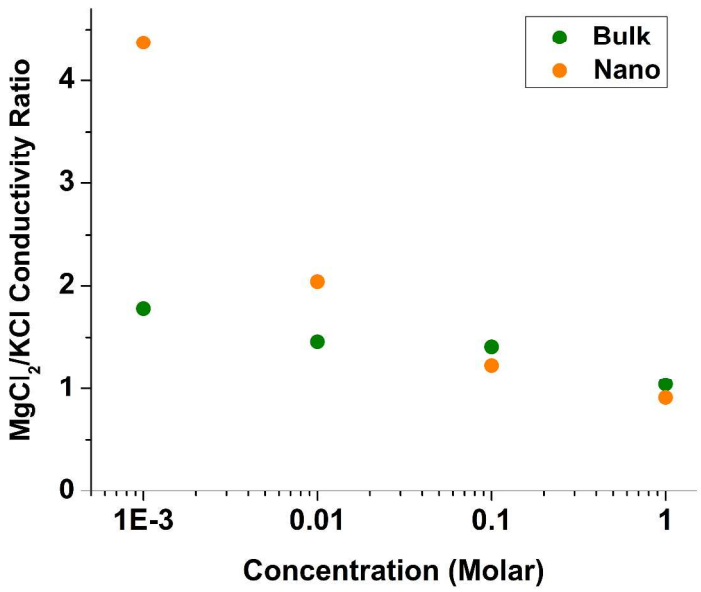


Figure S7

Figure S7: Divalent/Monovalent conductivity ratio plotted against concentration

6. Strongly Correlated Liquid Theory

A widely discussed explanation for the counter-intuitive phenomenon of charge inversion is the Strongly Correlated Liquid (SCL) theory proposed by Shklovskii, in which electrostatic correlations dominate. [3] When the bare surface charge is large enough and counterions have valence >=2, the repulsion between multivalent counterions at the interface is so strong that a strongly correlated two-dimensional layer is formed with a short-range order similar to Wigner Crystal. The SCL layer is characterized by a large negative chemical potential and attracts additional counterions to the surface due to the lateral correlations. Outside the SCL layer, the gaslike dilute phase of solution still can be explained by mean-field theories. If the electrochemical potentials of the SCL layer and the dilute phase are in equilibrium, the critical concentration of charge inversion equals:

$$C_0 = \frac{n}{w}\exp(-\frac{|\mu_c|}{k_B T})$$

Here $n = \sigma_{bare}/Ze$ and μ_c is the contribution of correlation to the chemical potential. We use a different w=0.8nm from the original 0.3nm, due to the unique hydrated structure of Mg^{2+} in water. Hydrated magnesium has a large average

diameter of 0.8nm, whereas hydrated potassium has an average diameter of 0.3nm. [4] It is also more difficult for hydrated Mg^{2+} ions to lose the water molecules around them, which will significantly influence the density and spatial arrangement of counterions at the surface. The calculated critical concentration for Mg^{2+} using the above equation is between 5mM and 38mM, depending on the bare surface charge. The accurate bare surface charge, however, is hard to estimate, due to the coupling effect of charge inversion and surface chemistry. The experimentally observed critical concentration of ~10mM $MgCl_2$ solution does fall in the range of theoretical estimation.

Reference:
1) Iller, Ralph K., The Chemistry of Silica. 1979
2) Duan, C. and A. Majumdar, Anomalous ion transport in 2-nm hydrophilic nanochannels. Nat. Nanotechnol., 2010. 5(12): p. 848-52.
3) Shklovskii, B.I., Screening of a macroion by multivalent ions: Correlation-induced inversion of charge. Phys. Rev. E, 1999. 60(5): p. 5802-5811.
4) Skoog, D.A. and D.M. West, Fundamentals of Analytical Chemistry, 4th edition, 1982